

Enhanced Black-Hole Mergers in Binary-Binary Interactions

Bin Liu^{1,2}, Dong Lai^{1,2,3}

¹ *Cornell Center for Astrophysics and Planetary Science, Cornell University, Ithaca, NY 14853, USA*

² *Shanghai Astronomical Observatory, Chinese Academy of Sciences, 80Nandan Road, Shanghai 200030, China*

³ *Tsung-Dao Lee Institute, Shanghai 200240, China*

8 March 2021

ABSTRACT

We study the orbital evolution of black hole (BH) binaries in quadruple systems, where the tertiary binary excites large eccentricity in the BH binary through Lidov-Kozai (LK) oscillations, causing the binary BHs to merge via gravitational radiation. For typical BH binaries with masses $m_{1,2} \simeq 20M_{\odot} - 30M_{\odot}$ and initial semimajor axis $a_0 \sim 100$ AU (such that the binaries have no chance of merging by themselves within $\sim 10^{10}$ yrs), we show that binary-binary interactions can significantly increase the LK window for mergers (the range of companion inclinations that allows the BH binary to merge within 10 Gyrs). This increase arises from a secular resonance between the LK oscillation of the BH binary and the nodal precession of the outer (binary-binary) orbit driven by the tertiary binary. Therefore, in the presence of tertiary binary, the BH merger fraction is increased to 10–30%, an order of magnitude larger than the merger fraction found in similar triple systems. Our analysis (with appropriate scalings) can be easily adapted to other configurations of systems, such as relatively compact BH binaries and moderately hierarchical triples, which may generate even higher merger fractions. Since the occurrence rate of stellar quadruples in the galactic fields is not much smaller than that of stellar triples, our result suggests that dynamically induced BH mergers in quadruple systems may be an important channel of producing BH mergers observed by LIGO/VIRGO.

Key words: binaries: general - black hole physics - gravitational waves - stars: black holes - stars: kinematics and dynamics

1 INTRODUCTION

Since 2015, a number of black hole (BH) binary and neutron star (NS) binary mergers have been observed in gravitational waves by aLIGO/VIRGO (e.g., Abbott et al. 2016a,b, 2017a,b,c,d). To bring two BHs into sufficiently close orbits and allow gravitational-radiation driven binary coalescence, several different formation scenarios have been proposed. These include isolated binary evolution, either through common-envelope phases (e.g., Lipunov et al. 1997, 2017; Podsiadlowski et al. 2003; Belczynski et al. 2010, 2016; Dominik et al. 2012, 2013, 2015) or through chemically homogeneous evolution associated with rapid stellar rotations (e.g., Mandel & de Mink 2016; Marchant et al. 2016), three-body encounters and/or secular interactions in dense star clusters such as globular cluster (e.g., Portegies Zwart &

McMillan 2000; Miller & Hamilton 2002; Wen 2003; Miller & Lauburg 2009; O’Leary et al. 2006; Banerjee et al. 2010; Downing et al. 2010; Thompson 2011; Rodriguez et al. 2015; Chatterjee et al. 2017; Samsing et al. 2018) or galactic nuclei (e.g., O’Leary et al. 2009; Antonini & Perets 2012; Antonini & Rasio 2016; VanLandingham et al. 2016; Petrovich & Antonini 2017; Hoang et al. 2018; Leigh et al. 2018), and secular/nonsecular Lidov-Kozai oscillations (e.g., Lidov 1962; Kozai 1962; Naoz 2016) in isolated triples in the galactic fields (e.g., Silsbee & Tremaine 2017; Antonini et al. 2017; Liu & Lai 2018).

The BH binary merger rate inferred from the LIGO detections ($10\text{--}200 \text{ Gpc}^{-3}\text{yr}^{-1}$) is higher than expected and challenges existing models. Additional mechanisms/effects may be required to produce a greater BH merger rate to match observations. Lidov-Kozai (LK) oscillations driven by

tertiary companions (either another star/BH in the galactic triple scenario, or a supermassive BH for binaries near galactic nuclei) provide a natural, purely dynamical mechanism to induce binary BH merger (e.g., Miller & Hamilton 2002; Wen 2003; Thompson 2011; Antonini & Perets 2012; Antonini et al. 2014; Hoang et al. 2018). In a recent paper (Liu & Lai 2018), we systematically study the merger window (the range of companion inclinations that allows the inner binary to merge within ~ 10 Gyrs) and merger fraction for BH binaries in triples for a wide range of parameters, taking account of both (octupole-level) secular and non-secular effects. We find that for a “typical” inner binary system (with masses $m_1 = 30M_\odot$, $m_2 = 20M_\odot$, initial separation $a_{\text{in}} = 100$ AU)¹ and a random orientation of the tertiary binary orbits, the merger fraction ranges from $\sim 1\%$ at $e_{\text{out}} = 0$ (quadrupole LK effect) to $\sim 10 - 20\%$ at $e_{\text{out}} = 0.9$ (octupole LK effect).

The merger fraction of BH binaries in triples can increase when the tertiary companion is a binary by itself (see Figure 1). Such binary-binary systems may allow Lidov-Kozai (LK) eccentricity excitation to operate over a wide range of inclinations (e.g., Pejcha et al. 2013; Vokrouhlický 2016; Hamers & Portegies Zwart 2016). The qualitative reason is as follows (Hamers & Lai 2017): the second binary induces nodal precession of the outer binary (at the characteristic rate Ω_{out}); when Ω_{out} matches the LK rate of the first (inner) binary, a secular resonance occurs; this can generate large mutual inclinations (between the first binary and the outer binary), and therefore induce eccentricity excitation of the first (inner) binary. Fang et al. (2018) and Hamers (2018a) studied this “enhanced LK effect” in the context of white dwarf (WD) binaries, with emphasis on WD-WD mergers relevant to Type Ia supernovae. Petrovich & Antonini (2017) considered a similar effect where stellar-mass BH binaries merging around a supermassive BH are embedded in a non-spherical galactic potential. They found that extreme eccentricity excitation is possible if the LK timescale driven by the central massive BH is comparable to the nodal precession timescale of the binary centre of mass driven by the non-spherical potential. An enhanced merger rate may also be achieved due to the effect of vector resonant relaxation of BH binaries in galactic nuclei (Hamers et al. 2018b).

In this paper, we study binary BH mergers in quadruple systems (Figure 1), focusing on the initially wide (~ 100 AU) BH binaries as in Liu & Lai (2018). We show that binary-binary interactions increase the LK window for extreme eccentricity excitations, and therefore significantly increase the BH binary merger fraction. We quantify the pa-

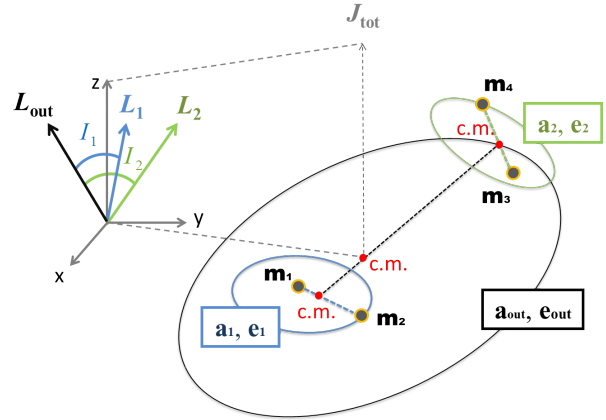


Figure 1. Illustration of the binary-binary system. The first (inner) binary is comprised of two BHs (m_1 and m_2); the second binary consists of another two bodies (m_3 and m_4) and orbits the center mass of the first inner binary, constituting the outer orbit. Here, $a_{1,2,\text{out}}$ are the semi-major axes, $e_{1,2,\text{out}}$ are the eccentricities of each binary. The total angular momentum $\mathbf{J}_{\text{tot}} = \mathbf{L}_1 + \mathbf{L}_2 + \mathbf{L}_{\text{out}}$ is along the z -axis, where \mathbf{L}_1 , \mathbf{L}_2 and \mathbf{L}_{out} (not to scale) denote the angular momenta of the first, second (inner) binaries and outer orbit, respectively, “c.m.” indicates the center of mass of each system. I_1 and I_2 are the mutual inclinations between \mathbf{L}_1 and \mathbf{L}_{out} , \mathbf{L}_2 and \mathbf{L}_{out} , respectively.

parameter space (e.g., the orbital properties of the tertiary binary) where this increase occurs. Our result suggests that although the quadruple stellar systems may not be as common as triples (e.g., Sana 2017), they could be the dominant sources for dynamically enhanced BH mergers in the galactic field.

Our paper is organized as follows. In Section 2, we summarize the secular equations of motion in the octupole order to evolve the quadruple systems with gravitational reaction. These equations are based on the double-averaged approximation (averaging over both inner and outer orbits) for the orbital evolution of hierarchical quadruple systems. In Section 3, we present the basic properties of LK oscillations for general stellar quadruples. In Section 4, we perform a suite of numerical integrations to determine the merger windows for LK-induced binary mergers, assuming isotropic distribution of the orientations of tertiary binaries. The associated merger fractions of BH binaries are then obtained. We summarize our main results in Section 5.

2 OCTUPOLE-LEVEL EQUATIONS OF MOTION FOR BINARY-BINARY SYSTEMS

We consider a hierarchical quadruple system, composed of two binaries orbiting each other, as depicted in Figure 1. The first (inner) BH binary has the masses m_1 , m_2 and the distant second (inner) binary has the masses m_3 and m_4 . The reduced mass for the first binary is $\mu_1 \equiv m_1 m_2 / m_{12}$, with $m_{12} \equiv m_1 + m_2$ and the second binary has $\mu_2 \equiv m_3 m_4 / m_{34}$, with $m_{34} \equiv m_3 + m_4$. The outer binary (m_{12} orbits around m_{34}) has $\mu_{\text{out}} \equiv (m_{12} m_{34}) / m_{\text{tot}}$ with $m_{\text{tot}} \equiv m_{12} + m_{34}$.

¹ Note that in the isolated binary evolution scenario, the massive stellar binaries must be formed with relatively small separations ($\lesssim 10$ AU), so that binary interactions (mass transfer and common envelop evolution) can shrink the orbit (e.g., Belczynski et al. 2016). Thus, we consider BH binaries with initially wider separations that cannot merge within the age of universe by themselves.

The semi-major axes and eccentricities are denoted by a_1 , a_2 , a_{out} and e_1 , e_2 , e_{out} , respectively. The orbital angular momenta of three orbits are

$$\mathbf{L}_1 = L_1 \hat{\mathbf{L}}_1 = \mu_1 \sqrt{Gm_{12}a_1(1 - e_1^2)} \hat{\mathbf{L}}_1, \quad (1)$$

$$\mathbf{L}_2 = L_2 \hat{\mathbf{L}}_2 = \mu_2 \sqrt{Gm_{34}a_2(1 - e_2^2)} \hat{\mathbf{L}}_2, \quad (2)$$

$$\mathbf{L}_{\text{out}} = L_{\text{out}} \hat{\mathbf{L}}_{\text{out}} = \mu_{\text{out}} \sqrt{Gm_{\text{tot}}a_{\text{out}}(1 - e_{\text{out}}^2)} \hat{\mathbf{L}}_{\text{out}}, \quad (3)$$

where $\hat{\mathbf{L}}_1$, $\hat{\mathbf{L}}_2$ and $\hat{\mathbf{L}}_{\text{out}}$ are unit vectors. We also define the eccentricity vectors as $\mathbf{e}_1 = e_1 \hat{\mathbf{e}}_1$, $\mathbf{e}_2 = e_2 \hat{\mathbf{e}}_2$ and $\mathbf{e}_{\text{out}} = e_{\text{out}} \hat{\mathbf{e}}_{\text{out}}$. For simplicity, we only study the LK-induced orbital decay in the first inner binary, considering the second one as an external perturber. Thus, for convenience of notation, we will frequently omit the subscript “1” for the first inner binary.

The secular equations of motion for the two inner binaries take the form:

$$\frac{d\mathbf{L}}{dt} = \left. \frac{d\mathbf{L}}{dt} \right|_{\text{LK}} + \left. \frac{d\mathbf{L}}{dt} \right|_{\text{GW}}, \quad (4)$$

$$\frac{d\mathbf{e}}{dt} = \left. \frac{d\mathbf{e}}{dt} \right|_{\text{LK}} + \left. \frac{d\mathbf{e}}{dt} \right|_{\text{GR}} + \left. \frac{d\mathbf{e}}{dt} \right|_{\text{GW}}, \quad (5)$$

$$\frac{dL_2}{dt} = \left. \frac{dL_2}{dt} \right|_{\text{LK}}, \quad (6)$$

$$\frac{de_2}{dt} = \left. \frac{de_2}{dt} \right|_{\text{LK}} + \left. \frac{de_2}{dt} \right|_{\text{GR}}, \quad (7)$$

and the outer orbit follows

$$\frac{d\mathbf{L}_{\text{out}}}{dt} = \left. \frac{d\mathbf{L}_{\text{out}}}{dt} \right|_{1\text{st}} + \left. \frac{d\mathbf{L}_{\text{out}}}{dt} \right|_{2\text{nd}}, \quad (8)$$

$$\frac{d\mathbf{e}_{\text{out}}}{dt} = \left. \frac{d\mathbf{e}_{\text{out}}}{dt} \right|_{1\text{st}} + \left. \frac{d\mathbf{e}_{\text{out}}}{dt} \right|_{2\text{nd}}. \quad (9)$$

In the first binary, we include the contributions from the outer binary (with perturber mass m_{34}) that generate LK oscillations (subscripted by “LK”), the general relativistic (GR) post-Newtonian correction, and the dissipation due to gravitational wave (GW) emission (see Equations 4-5). We also evolve the second binary throughout the paper as the first one but without the GW radiation (Equations 6-7). The outer binary’s angular momentum and eccentricity are affected by Newtonian potential from both the first and second inner binaries (subscripted by “1st” and “2nd”).

To describe the LK oscillations, we introduce the reduced angular momentum vectors as

$$\mathbf{j} \equiv j \hat{\mathbf{L}} = \sqrt{1 - e^2} \hat{\mathbf{L}}, \quad (10)$$

$$\mathbf{j}_{\text{out}} \equiv j_{\text{out}} \hat{\mathbf{L}}_{\text{out}} = \sqrt{1 - e_{\text{out}}^2} \hat{\mathbf{L}}_{\text{out}}. \quad (11)$$

Therefore, for the first binary, we have, to the octupole order

(Liu et al. 2015; Petrovich 2015)

$$\begin{aligned} \left. \frac{d\mathbf{j}}{dt} \right|_{\text{LK}} = & \frac{3}{4 t_{\text{LK},12}} \left[(\mathbf{j} \cdot \hat{\mathbf{L}}_{\text{out}}) \mathbf{j} \times \hat{\mathbf{L}}_{\text{out}} - 5(\mathbf{e} \cdot \hat{\mathbf{L}}_{\text{out}}) \mathbf{e} \times \hat{\mathbf{L}}_{\text{out}} \right] \\ & - \frac{75\varepsilon_{\text{oct},12}}{64 t_{\text{LK},12}} \left\{ \left[2 \left[(\mathbf{e} \cdot \hat{\mathbf{e}}_{\text{out}}) (\mathbf{j} \cdot \hat{\mathbf{L}}_{\text{out}}) \right. \right. \right. \\ & + (\mathbf{e} \cdot \hat{\mathbf{L}}_{\text{out}}) (\mathbf{j} \cdot \hat{\mathbf{e}}_{\text{out}}) \left. \right] \mathbf{j} + 2 \left[(\mathbf{j} \cdot \hat{\mathbf{e}}_{\text{out}}) (\mathbf{j} \cdot \hat{\mathbf{L}}_{\text{out}}) \right. \\ & - 7(\mathbf{e} \cdot \hat{\mathbf{e}}_{\text{out}}) (\mathbf{e} \cdot \hat{\mathbf{L}}_{\text{out}}) \left. \right] \mathbf{e} \left. \right\} \times \hat{\mathbf{L}}_{\text{out}} \\ & + \left[2(\mathbf{e} \cdot \hat{\mathbf{L}}_{\text{out}}) (\mathbf{j} \cdot \hat{\mathbf{L}}_{\text{out}}) \mathbf{j} + \left[\frac{8}{5} e^2 - \frac{1}{5} \right. \right. \\ & \left. \left. - 7(\mathbf{e} \cdot \hat{\mathbf{L}}_{\text{out}})^2 + (\mathbf{j} \cdot \hat{\mathbf{L}}_{\text{out}})^2 \right] \mathbf{e} \right] \times \hat{\mathbf{e}}_{\text{out}} \left. \right\}, \quad (12) \end{aligned}$$

and

$$\begin{aligned} \left. \frac{d\mathbf{e}}{dt} \right|_{\text{LK}} = & \frac{3}{4 t_{\text{LK},12}} \left[(\mathbf{j} \cdot \hat{\mathbf{L}}_{\text{out}}) \mathbf{e} \times \hat{\mathbf{L}}_{\text{out}} + 2 \mathbf{j} \times \mathbf{e} \right. \\ & \left. - 5(\mathbf{e} \cdot \hat{\mathbf{L}}_{\text{out}}) \mathbf{j} \times \hat{\mathbf{L}}_{\text{out}} \right] \\ & - \frac{75\varepsilon_{\text{oct},12}}{64 t_{\text{LK},12}} \left\{ \left[2(\mathbf{e} \cdot \hat{\mathbf{L}}_{\text{out}}) (\mathbf{j} \cdot \hat{\mathbf{L}}_{\text{out}}) \mathbf{e} \right. \right. \\ & + \left[\frac{8}{5} e^2 - \frac{1}{5} - 7(\mathbf{e} \cdot \hat{\mathbf{L}}_{\text{out}})^2 + (\mathbf{j} \cdot \hat{\mathbf{L}}_{\text{out}})^2 \right] \mathbf{j} \left. \right\} \times \hat{\mathbf{e}}_{\text{out}} \\ & + \left[2 \left[(\mathbf{e} \cdot \hat{\mathbf{e}}_{\text{out}}) (\mathbf{j} \cdot \hat{\mathbf{L}}_{\text{out}}) + (\mathbf{e} \cdot \hat{\mathbf{L}}_{\text{out}}) (\mathbf{j} \cdot \hat{\mathbf{e}}_{\text{out}}) \right] \mathbf{e} \right. \\ & + 2 \left[(\mathbf{j} \cdot \hat{\mathbf{L}}_{\text{out}}) (\mathbf{j} \cdot \hat{\mathbf{e}}_{\text{out}}) - 7(\mathbf{e} \cdot \hat{\mathbf{L}}_{\text{out}}) (\mathbf{e} \cdot \hat{\mathbf{e}}_{\text{out}}) \right] \mathbf{j} \left. \right\} \times \hat{\mathbf{L}}_{\text{out}} \\ & + \frac{16}{5} (\mathbf{e} \cdot \hat{\mathbf{e}}_{\text{out}}) \mathbf{j} \times \mathbf{e} \left. \right\}, \quad (13) \end{aligned}$$

where

$$\varepsilon_{\text{oct},12} \equiv \frac{m_1 - m_2}{m_{12}} \left(\frac{a}{a_{\text{out}}} \right) \frac{e_{\text{out}}}{1 - e_{\text{out}}^2} \quad (14)$$

measures the relative strength of the octupole potential compared to the quadrupole one. The quadrupole term induces the oscillations in the eccentricity and mutual orbital inclination on the timescale of

$$t_{\text{LK},12} = \frac{1}{n} \frac{m_{12}}{m_{34}} \left(\frac{a_{\text{out,eff}}}{a} \right)^3, \quad (15)$$

where $n = (Gm_{12}/a^3)^{1/2}$ is the mean motion of the first inner binary and the effective outer binary separation is defined as

$$a_{\text{out,eff}} \equiv a_{\text{out}} \sqrt{1 - e_{\text{out}}^2}. \quad (16)$$

General Relativity (1-PN correction) introduces pericenter precession as

$$\left. \frac{d\mathbf{e}}{dt} \right|_{\text{GR}} = \Omega_{\text{GR}} \hat{\mathbf{L}} \times \mathbf{e}, \quad (17)$$

with the precession rate given by

$$\Omega_{\text{GR}} = \frac{3Gnm_{12}}{c^2 a(1 - e^2)}, \quad (18)$$

Gravitational radiation draws energy and angular momentum from the BH orbit. The rates of change of \mathbf{L} and

\mathbf{e} are (Peters 1964)

$$\frac{d\mathbf{L}}{dt}\Big|_{\text{GW}} = -\frac{32}{5} \frac{G^{7/2}}{c^5} \frac{\mu^2 m_{12}^{5/2}}{a^{7/2}} \frac{1+7e^2/8}{(1-e^2)^2} \hat{\mathbf{L}}, \quad (19)$$

$$\frac{d\mathbf{e}}{dt}\Big|_{\text{GW}} = -\frac{304}{15} \frac{G^3}{c^5} \frac{\mu m_{12}^2}{a^4 (1-e^2)^{5/2}} \left(1 + \frac{121}{304} e^2\right) \mathbf{e}. \quad (20)$$

The merger time due to GW radiation of an isolated binary with the initial semi-major axis a_0 and eccentricity $e_0 = 0$ is given by

$$T_{\text{m},0} = \frac{5c^5 a_0^4}{256G^3 m_{12}^2 \mu} \quad (21)$$

$$\simeq 10^{10} \left(\frac{60M_\odot}{m_{12}}\right)^2 \left(\frac{15M_\odot}{\mu}\right) \left(\frac{a_0}{0.202\text{AU}}\right)^4 \text{ yrs.}$$

In our calculations, we also evolve the second binary, except that we do not include the GW terms for the sake of clarity. By switching the indices $\mathbf{j} \rightarrow \mathbf{j}_2$, $\mathbf{e} \rightarrow \mathbf{e}_2$, $\varepsilon_{\text{oct},34}$ and $t_{\text{LK},34}$, Equations (12)-(13) and (17) can be applied to the second binary (with $m_1 \rightarrow m_3$, $m_2 \rightarrow m_4$, $m_{12} \rightarrow m_{34}$, $a \rightarrow a_2$ and $n \rightarrow (Gm_{34}/a_2^3)^{1/2}$ in Equations 14-15, 18). The outer orbit is influenced by both first and second binary. The first piece of Equation (8) is given by

$$\begin{aligned} \frac{d\mathbf{j}_{\text{out}}}{dt}\Big|_{1\text{st}} &= \frac{3}{4t_{\text{LK},12}} \frac{\Lambda}{\Lambda_{\text{out}}} \left[(\mathbf{j} \cdot \hat{\mathbf{L}}_{\text{out}}) \hat{\mathbf{L}}_{\text{out}} \times \mathbf{j} \right. \\ &- 5(\mathbf{e} \cdot \hat{\mathbf{L}}_{\text{out}}) \hat{\mathbf{L}}_{\text{out}} \times \mathbf{e} \\ &- \frac{75\varepsilon_{\text{oct},12}}{64t_{\text{LK},12}} \frac{\Lambda}{\Lambda_{\text{out}}} \left\{ 2 \left[(\mathbf{e} \cdot \hat{\mathbf{L}}_{\text{out}})(\mathbf{j} \cdot \hat{\mathbf{e}}_{\text{out}}) \hat{\mathbf{L}}_{\text{out}} \right. \right. \\ &+ (\mathbf{e} \cdot \hat{\mathbf{e}}_{\text{out}})(\mathbf{j} \cdot \hat{\mathbf{L}}_{\text{out}}) \hat{\mathbf{L}}_{\text{out}} + (\mathbf{e} \cdot \hat{\mathbf{L}}_{\text{out}})(\mathbf{j} \cdot \hat{\mathbf{L}}_{\text{out}}) \hat{\mathbf{e}}_{\text{out}} \left. \right] \times \mathbf{j} \\ &+ \left[2(\mathbf{j} \cdot \hat{\mathbf{e}}_{\text{out}})(\mathbf{j} \cdot \hat{\mathbf{L}}_{\text{out}}) \hat{\mathbf{L}}_{\text{out}} - 14(\mathbf{e} \cdot \hat{\mathbf{e}}_{\text{out}})(\mathbf{e} \cdot \hat{\mathbf{L}}_{\text{out}}) \hat{\mathbf{L}}_{\text{out}} \right. \\ &\left. \left. + \left[\frac{8}{5}e^2 - \frac{1}{5} - 7(\mathbf{e} \cdot \hat{\mathbf{L}}_{\text{out}})^2 + (\mathbf{j} \cdot \hat{\mathbf{L}}_{\text{out}})^2 \right] \hat{\mathbf{e}}_{\text{out}} \right] \times \mathbf{e} \right\} \end{aligned} \quad (22)$$

The evolution equation of \mathbf{L}_{out} is $(d\mathbf{L}_{\text{out}}/dt)|_{1\text{st}} =$

$\mu_{\text{out}} \sqrt{Gm_{\text{tot}} a_{\text{out}}} (d\mathbf{j}_{\text{out}}/dt)|_{1\text{st}}$. Also

$$\begin{aligned} \frac{d\mathbf{e}_{\text{out}}}{dt}\Big|_{1\text{st}} &= \frac{3}{4t_{\text{LK},12} \sqrt{1-e_{\text{out}}^2}} \frac{\Lambda}{\Lambda_{\text{out}}} \left[(\mathbf{j} \cdot \hat{\mathbf{L}}_{\text{out}}) \mathbf{e}_{\text{out}} \times \mathbf{j} \right. \\ &- 5(\mathbf{e} \cdot \hat{\mathbf{L}}_{\text{out}}) \mathbf{e}_{\text{out}} \times \mathbf{e} - \left[\frac{1}{2} - 3e^2 + \frac{25}{2} (\mathbf{e} \cdot \hat{\mathbf{L}}_{\text{out}})^2 \right. \\ &- \left. \left. \frac{5}{2} (\mathbf{j} \cdot \hat{\mathbf{L}}_{\text{out}})^2 \right] \hat{\mathbf{L}}_{\text{out}} \times \mathbf{e}_{\text{out}} \right] - \frac{75}{64t_{\text{LK},12}} \frac{\varepsilon_{\text{oct},12}}{\sqrt{1-e_{\text{out}}^2}} \frac{\Lambda}{\Lambda_{\text{out}}} \\ &\times \left\{ 2 \left[(\mathbf{e} \cdot \hat{\mathbf{L}}_{\text{out}})(\mathbf{j} \cdot \mathbf{e}_{\text{out}}) \hat{\mathbf{e}}_{\text{out}} + (\mathbf{j} \cdot \hat{\mathbf{L}}_{\text{out}})(\mathbf{e} \cdot \mathbf{e}_{\text{out}}) \hat{\mathbf{e}}_{\text{out}} \right. \right. \\ &+ \frac{1-e_{\text{out}}^2}{e_{\text{out}}} (\mathbf{e} \cdot \hat{\mathbf{L}}_{\text{out}})(\mathbf{j} \cdot \hat{\mathbf{L}}_{\text{out}}) \hat{\mathbf{L}}_{\text{out}} \left. \right] \times \mathbf{j} \\ &+ \left[2(\mathbf{j} \cdot \mathbf{e}_{\text{out}})(\mathbf{j} \cdot \hat{\mathbf{L}}_{\text{out}}) \hat{\mathbf{e}}_{\text{out}} - 14(\mathbf{e} \cdot \mathbf{e}_{\text{out}})(\mathbf{e} \cdot \hat{\mathbf{L}}_{\text{out}}) \hat{\mathbf{e}}_{\text{out}} \right. \\ &+ \frac{1-e_{\text{out}}^2}{e_{\text{out}}} \left[\frac{8}{5}e^2 - \frac{1}{5} - 7(\mathbf{e} \cdot \hat{\mathbf{L}}_{\text{out}})^2 \right. \\ &+ (\mathbf{j} \cdot \hat{\mathbf{L}}_{\text{out}})^2 \left. \right] \hat{\mathbf{L}}_{\text{out}} \left. \right] \times \mathbf{e} - \left[2 \left(\frac{1}{5} - \frac{8}{5}e^2 \right) (\mathbf{e} \cdot \hat{\mathbf{e}}_{\text{out}}) \mathbf{e}_{\text{out}} \right. \\ &+ 14(\mathbf{e} \cdot \hat{\mathbf{L}}_{\text{out}})(\mathbf{j} \cdot \hat{\mathbf{e}}_{\text{out}})(\mathbf{j} \cdot \hat{\mathbf{L}}_{\text{out}}) \mathbf{e}_{\text{out}} \\ &+ 7(\mathbf{e} \cdot \hat{\mathbf{e}}_{\text{out}}) \left[\frac{8}{5}e^2 - \frac{1}{5} - 7(\mathbf{e} \cdot \hat{\mathbf{L}}_{\text{out}})^2 \right. \\ &\left. \left. + (\mathbf{j} \cdot \hat{\mathbf{L}}_{\text{out}})^2 \right] \mathbf{e}_{\text{out}} \right] \times \hat{\mathbf{L}}_{\text{out}} \left. \right\}. \quad (23) \end{aligned}$$

Here, we have defined

$$\Lambda \equiv L|_{e=0} = \mu \sqrt{Gm_{12}a}, \quad (24)$$

$$\Lambda_{\text{out}} \equiv L_{\text{out}}|_{e_{\text{out}}=0} = \mu_{\text{out}} \sqrt{Gm_{\text{tot}}a_{\text{out}}}. \quad (25)$$

Similar expressions apply to $(d\mathbf{j}_{\text{out}}/dt)|_{2\text{nd}}$ and $(d\mathbf{e}_{\text{out}}/dt)|_{2\text{nd}}$. Equations (4)-(9) completely determine the secular evolution of the binary-binary system. These equations are based on the double averaging approximation, and require that the timescale near the maximum eccentricity e_{max} be longer than the period of the outer binary (e.g., Seto 2013; Antonini et al. 2014), i.e.

$$t_{\text{LK}} \sqrt{1-e_{\text{max}}^2} \gtrsim P_{\text{out}}. \quad (26)$$

See Liu & Lai (2018) for more discussion on the regime of validity of the double-averaged equations and the more general single-averaged equations.

3 EXCITATION OF ECCENTRICITY IN BINARY-BINARY SYSTEMS

Before considering the population of binary mergers in quadruple systems (Section 4), we first examine how binary-binary interaction influences the excitation of eccentricity in the inner binary.

Figure 2 shows the maximum excited eccentricity achieved in the first binary (e_{max} ; in the absence of GW emission) and merger window (including GW emission; to be discussed in Section 4) as a function of the initial mutual inclination angle I_0 (the initial value of I_1). The binary has masses $m_1 = 30M_\odot$, $m_2 = 20M_\odot$, and the initial semimajor axis $a_0 = 100\text{AU}$ and the initial eccentricity

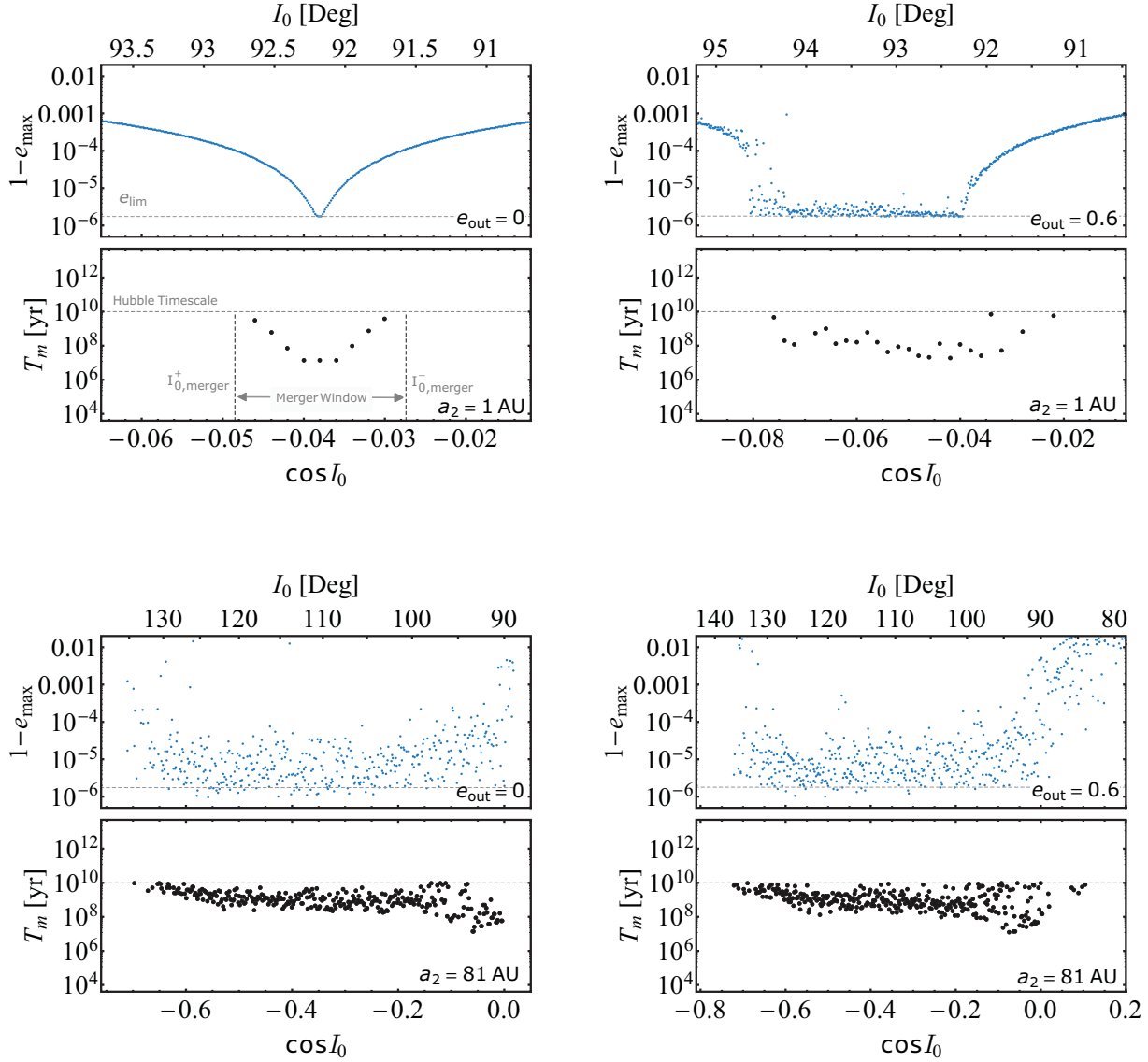


Figure 2. Eccentricity excitation and merger window in binary-binary systems for different values of e_{out} and a_2 . In each panel, the upper and lower plots show the maximum eccentricity e_{max} (assuming no GW emission) and the first (inner) binary merger time T_m (with GW emission) as a function of I_0 (the initial value of I_1). The system parameters are: $m_1 = 30M_\odot$, $m_2 = 20M_\odot$, $a_0 = 100\text{AU}$ (initial value of a), $e_0 = e_{2,0} = 0.001$, $m_3 = m_4 = 15M_\odot$, $a_{\text{out}} = 4400\text{AU}$ (for $e_{\text{out}} = 0$) and $a_{\text{out}} = 5500\text{AU}$ (for $e_{\text{out}} = 0.6$). The longitude of the periaapse $\omega_{\text{out},0}$ is randomly chosen in the range of $(0, 2\pi)$. All four panels have the same $\bar{a}_{\text{out,eff}} = 4.4$ (Equation 27), implying the same quadrupolar perturbation strength from the second tertiary binary, and the double-averaged secular approximation can be safely satisfied (Equation 26). Each black dot (obtained by solving Equations 4-9) represents a successful merger event within 10^{10} yrs (note that the grid of blue dots is denser than the black dots). The dashed horizontal line (e_{lim}) is given by Equation (30).

$e_0 = 0$. As noted before (see footnote 1), such binaries cannot merge by themselves with tertiary companions. For simplicity, we choose the second binary to have equal masses, i.e., $m_3 = m_4 = 15M_\odot$ and circular orbit at $t = 0$ ($e_{2,0} = 0$). Note that the unequal masses in the second binary can induce the similar behaviors as the first binary, where the octupole contribution comes into play. In this situation, both the evolution of $\hat{\mathbf{L}}_2$ and $\hat{\mathbf{L}}_{\text{out}}$ might become chaotic, which in turn could widen the window of e -excitation in the first inner binary. The properties of the dynamics is beyond the scope of this paper and we leave it to a future work. Here, we

integrate the Equations (4)-(9) and fix the initial inclination of the second binary to be $I_{2,0} = 30^\circ$, so that no LK oscillations occur in the second binary, and we concentrate on the eccentricity excitation of the first binary. As in Liu & Lai (2018), we introduce the effective outer binary semimajor axis as $a_{\text{out,eff}} = a_{\text{out}} \sqrt{1 - e_{\text{out}}^2}$ and define

$$\begin{aligned} \bar{a}_{\text{out,eff}} &\equiv \left(\frac{a_{\text{out,eff}}}{1000\text{AU}} \right) \left(\frac{m_{34}}{30M_\odot} \right)^{-1/3} \\ &= \left(\frac{a_{\text{out}} \sqrt{1 - e_{\text{out}}^2}}{1000\text{AU}} \right) \left(\frac{m_{34}}{30M_\odot} \right)^{-1/3}. \end{aligned} \quad (27)$$

This quantity characterizes the “quadrupole strength” of the outer perturber $m_{34} = m_3 + m_4$. In the examples depicted in Figure 2, we adopt $\bar{a}_{\text{out,eff}} = 4.4$, where the double-averaged secular equations derived here can be safely used based on Equation (26) (where we replace e_{max} with e_{lim} ; see Equation 30). Thus, we have $a_{\text{out}} = 4400\text{AU}$ for $e_{\text{out}} = 0$ and $a_{\text{out}} = 5500\text{AU}$ for $e_{\text{out}} = 0.6$. The initial longitude of the periapse ω_{out} is randomly chosen in the range of $(0, 2\pi)$.

The top two panels of Figure 2 show the results when $a_2 \ll a_{\text{out}}$. In these cases, the binary-binary system effectively reduces to a triple system, with the first binary perturbed by m_{34} . When $e_{\text{out}} = 0$ (the top left panel of Figure 2), the octupole effect vanishes, and the maximum eccentricity e_{max} achieved by the first binary (starting from $e_0 \simeq 0$) can be evaluated analytically (Liu et al. 2015; Anderson et al. 2017):

$$\frac{3}{8} \frac{j_{\text{min}}^2 - 1}{j_{\text{min}}^2} \left[5 \left(\cos I_0 + \frac{\eta}{2} \right)^2 - \left(3 + 4\eta \cos I_0 + \frac{9}{4} \eta^2 \right) j_{\text{min}}^2 + \eta^2 j_{\text{min}}^4 \right] + \varepsilon_{\text{GR}} (1 - j_{\text{min}}^{-1}) = 0, \quad (28)$$

where $j_{\text{min}} \equiv \sqrt{1 - e_{\text{max}}^2}$, $\eta \equiv (L/L_{\text{out}})_{e=0}$, and

$$\varepsilon_{\text{GR}} = \frac{3Gm_{12}^2 a_{\text{out,eff}}^3}{c^2 a^4 m_{34}} \simeq 3.6 \times 10^{-5} \left(\frac{m_{12}}{60M_{\odot}} \right)^2 \left(\frac{m_{34}}{30M_{\odot}} \right)^{-1} \left(\frac{a_{\text{out,eff}}}{10^3 \text{AU}} \right)^3 \left(\frac{a}{10^2 \text{AU}} \right)^{-4}, \quad (29)$$

which measures the strength of the GR precession (relative to the LK oscillations). Note that in the limit of $\eta \rightarrow 0$ and $\varepsilon_{\text{GR}} \rightarrow 0$, Equation (28) yields the well-known relation $e_{\text{max}} = \sqrt{1 - (5/3) \cos^2 I_0}$. The maximum possible e_{max} for all values of I_0 , called e_{lim} , is given by

$$\frac{3}{8} (j_{\text{lim}}^2 - 1) \left[-3 + \frac{\eta^2}{4} \left(\frac{4}{5} j_{\text{lim}}^2 - 1 \right) \right] + \varepsilon_{\text{GR}} (1 - j_{\text{lim}}^{-1}) = 0. \quad (30)$$

From the top panels of Figure 2 (with $a_2 = 1 \text{AU}$), we see that for $e_{\text{out}} = 0$, the limiting eccentricity can be achieved only in a very narrow inclination window around $I_0 = 92.2^\circ$. For $e_{\text{out}} = 0.6$ (corresponding to $\varepsilon_{\text{oct},12} \simeq 0.003$), the same limiting eccentricity applies (see Liu et al. 2015), but it can be achieved over a wide range of $I_0 \in [92^\circ, 94.5^\circ]$.

The lower panels of Figure 2 show e_{max} versus I_0 when the second binary has a semimajor axis $a_2 = 81\text{AU}$. We see that regardless of the value of e_{out} (i.e., the strength of the octupole potential), extreme eccentricity excitation can be achieved over a much wider range of inclinations, roughly from 90° to 130° .

The enhanced inclination range for LK oscillations in binary-binary systems can be understood as a resonance phenomenon (Hamers & Lai 2017). Considering the simple case where the second binary does not experience LK oscillation and stays circular ($e_2 = 0$) and the outer binary is also circular ($e_{\text{out}} = 0$). So, no octupole effect comes into play, and the angular momentum axis of the outer binary is

affected by the second binary via

$$\frac{d\hat{\mathbf{L}}_{\text{out}}}{dt} \Big|_{2\text{nd}} = \frac{3}{4t_{\text{LK},34}} \frac{L_2}{L_{\text{out}}} (\hat{\mathbf{L}}_2 \cdot \hat{\mathbf{L}}_{\text{out}}) \hat{\mathbf{L}}_{\text{out}} \times \hat{\mathbf{L}}_2, \quad (31)$$

where $t_{\text{LK},34}$ is the LK timescale in the second binary, given by

$$t_{\text{LK},34} = \frac{1}{n_2} \frac{m_{34}}{m_{12}} \left(\frac{a_{\text{out,eff}}}{a_2} \right)^3, \quad (32)$$

where $n_2 = (Gm_{34}/a_2^3)^{1/2}$. Thus, $\hat{\mathbf{L}}_{\text{out}}$ is driven into precession around the $\mathbf{L}_{2+\text{out}} \equiv \mathbf{L}_2 + \mathbf{L}_{\text{out}}$ axis at the rate

$$\Omega_{\text{out}} = \frac{3}{4t_{\text{LK},34}} \frac{|\mathbf{L}_2 + \mathbf{L}_{\text{out}}|}{L_{\text{out}}} (\hat{\mathbf{L}}_2 \cdot \hat{\mathbf{L}}_{\text{out}}) \simeq \frac{3}{4t_{\text{LK},34}} \cos I_2. \quad (33)$$

On the other hand, the outer binary drives LK oscillations of the (first) inner binary on timescale $t_{\text{LK},12}$. Thus, we define the dimensionless parameter

$$\beta \equiv \Omega_{\text{out}} t_{\text{LK},12} = \frac{3}{4} \cos I_2 \left(\frac{a_2}{a_1} \right)^{3/2} \left(\frac{m_1 + m_2}{m_3 + m_4} \right)^{3/2}. \quad (34)$$

The value of β measures the ratio between the LK timescale in the first binary and the precession timescale of the outer orbit. When $\beta \ll 1$, the second binary essentially acts like a single mass ($m_3 + m_4$), and “normal” LK oscillations apply. When $\beta \gg 1$, $\hat{\mathbf{L}}_{\text{out}}$ precesses rapidly around the $\mathbf{L}_{2+\text{out}}$, the problem again reduces to that of “normal” LK oscillations, with $\hat{\mathbf{L}}_{2+\text{out}}$ serving as the effective $\hat{\mathbf{L}}_{\text{out}}$. When $\beta \sim 1$, a secular resonance occurs that generates large I even for initially low-inclination systems, and this resonantly excited inclination then leads to LK oscillations of the inner binary.

In the lower panels of Figure 2, the parameters of the system (with $a_2 = 81\text{AU}$) gives $\beta \simeq 1$. So we indeed see that the width of LK window for extreme eccentricity excitation is significantly enhanced due to the presence of the tertiary binary. Note that the eccentricity of the inner binary can undergo excursions to more extreme values than the analytical prediction of e_{lim} . Also, when the outer binary is eccentric ($e_{\text{out}} = 0.6$), the octupole effect comes into play, and the LK window is further extended (although slightly). Overall, Figure 2 shows that the orbital properties of the second binary play a more important role compared to the octupole terms in exciting eccentricity of the first inner binary and largely determine the LK window.

4 MERGER WINDOW AND MERGER FRACTION

In this section, we study the LK oscillations including gravitational radiation for binary-binary systems. We evolve all the three binaries (using double-averaged secular equations presented in Section 2). To emphasize the role of the tertiary binary, we do not include the GW emission in the second binary and focus on the merger window of the first inner binary (i.e., the initial inclination I_0 that gives mergers in less than 10^{10} yrs). Note that similar behaviors are expected when GW radiation in the second binary is considered (if the

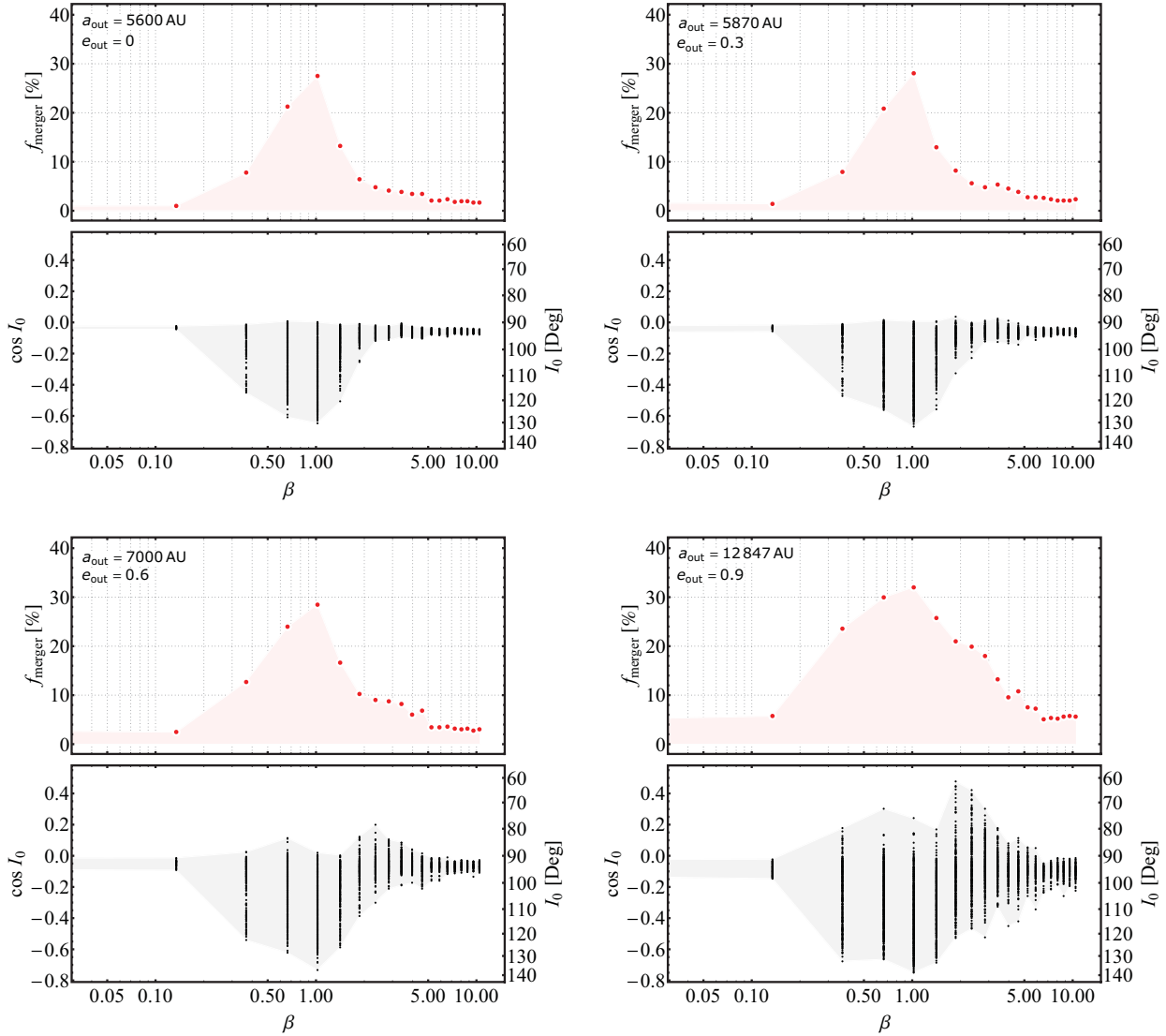


Figure 3. Merger fraction and merger window as a function of the dimensionless parameter β (Equation 34) for different values of a_{out} and e_{out} . The system parameters are $m_1 = 30M_{\odot}$, $m_2 = 20M_{\odot}$, $a_0 = 100\text{AU}$, $m_3 = m_4 = 15M_{\odot}$, and $e_0 = e_{2,0} = 0.001$. All four panels have the same $\bar{a}_{\text{out,eff}} = 5.6$ (Equation 27) and ω_{out} is initialized randomly in $(0, 2\pi)$. In each panel, the bottom plot shows the merger window with each dot representing a successful merger within 10 Gyrs; the top plot shows the merger fraction from the mergers shown in the bottom plot. The shaded areas highlight the boundaries of the resonance parameter regimes.

second binary lies in the eccentricity excitation window). In this case, the total merger rate is simply doubled.

First consider the examples shown in Figure 2. The upper two panels (with $a_2 = 1\text{AU}$, so that the second binary behaves like a single mass) correspond to the result already found in Liu & Lai (2018): the inner binary can merge within 10^{10} yrs only if its eccentricity is excited to sufficiently large value, and the merger window increases as the octupole effect (measured by ε_{oct}) becomes stronger. Note that for $\varepsilon_{\text{oct}} = 0$ and $(1 - e_{\text{max}}) \ll 1$, the merger window can be determined analytically: the merger time is given by

$$T_m \simeq T_{m,0}(1 - e_{\text{max}}^2)^3 \quad (35)$$

to a good approximation (see Equation 48 of Liu & Lai (2018) and regime of validity of this equation), with $T_{m,0}$

given by Equation (21). Combining Equations (28) and (35) and setting $T_m = 10^{10}$ yrs, the upper and lower boundaries of the merger window, $I_{0,\text{merger}}^{\pm}$, can be obtained.

The lower panels of Figure 2 show that for $\beta \simeq 1$, as a direct consequence of the widened LK eccentricity excitation window, the binary merger window also significantly widens compared to the case with small a_2 (or $\beta \ll 1$).

In order to systematically explore how the merger window and merger fraction vary for different binary-binary parameters, we carry out calculations for different values of β by changing a_2 . Due to the large uncertainties about the stellar quadrupole populations and their properties (see Sana 2017), we are not trying to perform the calculations including full population synthesis. Instead, we follow the fiducial

BH binaries in Figure 2 and survey all possible values of a_2 and a_{out} . We set $m_3 = m_4 = 15M_\odot$, but note that the mass of the second binary m_{34} is less relevant since it can be rescaled by Equation (16) (i.e., the combination of $a_{\text{out,eff}}$ and m_{34} determines the perturbation strength). For a given a_{out} and e_{out} , the semimajor axis of the second binary must satisfy the stability criterion of Mardling & Aarseth (2001):

$$\frac{a_{\text{out}}}{a_2} > 2.8 \left(1 + \frac{m_{12}}{m_{34}}\right)^{2/5} \frac{(1 + e_{\text{out}})^{2/5}}{(1 - e_{\text{out}})^{6/5}} \left(1 - \frac{0.3I_{2,0}}{180^\circ}\right). \quad (36)$$

Figure 3 shows the dependence of the merger fraction and merger window on β for several different semimajor axis of the outer binary, where $a_{\text{out}} = 5600\text{AU}$ ($e_{\text{out}} = 0$), $a_{\text{out}} = 5870\text{AU}$ ($e_{\text{out}} = 0.3$), $a_{\text{out}} = 7000\text{AU}$ ($e_{\text{out}} = 0.6$) and $a_{\text{out}} = 12847\text{AU}$ ($e_{\text{out}} = 0.9$), all given $\bar{a}_{\text{out,eff}} = 5.6$ (Equation 27) and satisfy with the double-averaged secular approximation (Equation 26). We see that the merger window indeed is much wider for $\beta \simeq 0.3 - 3$. This range is somewhat larger when the octupole effect (ε_{oct}) increases. Note that the initial mutual inclinations for successful mergers inside the merger window are not uniformly distributed. This is because the overlap of resonances from both binary-binary interactions (e.g., Hamers & Lai 2017) and octupole terms (e.g., Lithwick et al. 2011; Li et al. 2015) together induces chaos of the systems with intermediate β .

To calculate the merger fraction, we assume that the initial inclination of the outer binary is uniformly distributed in $\cos I_0 \in [-1, 1]$. As shown in Figure 3, f_{merger} exhibits a clear dependence on β . The secular resonance around $\beta \simeq 1$ gives the the maximum $f_{\text{merger}} \sim 30\%$, which is $\sim 6 - 30$ times larger than the cases with $\beta \ll 1$ (equivalent to a “pure” triple). We also see that compared to the octupole contribution, the resonance plays an more significant role in determining the merger fraction.

Equation (34) indicates that β has a dependence on I_2 . In the calculations shown above (Figures 2-3), the angular momentum vector of the second binary \mathbf{L}_2 is always placed initially at 30° with respect to \mathbf{L}_{out} . In Figure 4, we set the initial $I_{2,0}$ to 15° and 45° , and all other parameters are sampled identically to the case of $e_{\text{out}} = 0.6$ depicted in Figure 3. The different results for $I_{2,0} = 15^\circ$ and 45° arise from the fact that I_2 varies in time in the case of $I_{2,0} = 45^\circ$, giving rise to time-dependent β . Also, the amplitude of nodal precession of the outer binary (i.e., the angle between \mathbf{L}_{out} and \mathbf{L}_{tot}) for the two cases are different, and this difference can affect the LK oscillations of the first inner binary (see Hamers & Lai 2017).

To illustrate how the merger window and merger fraction depend on the properties of the outer binary, Figures 5-6 show our results as a function of $\bar{a}_{\text{out,eff}}$ for several values of β . This is similar to Figure 3, but shown in a different way. When $\beta \ll 1$, for a given e_{out} , the merger window shows an general trend of widening as $\bar{a}_{\text{out,eff}}$ decreases. Note that for $e_{\text{out}} \simeq 0$, the merger window (the dashed curve in each panel) and merger fraction can be obtained analytically using Equations (28) and (35) (see Equations 51, 53 and 54 of

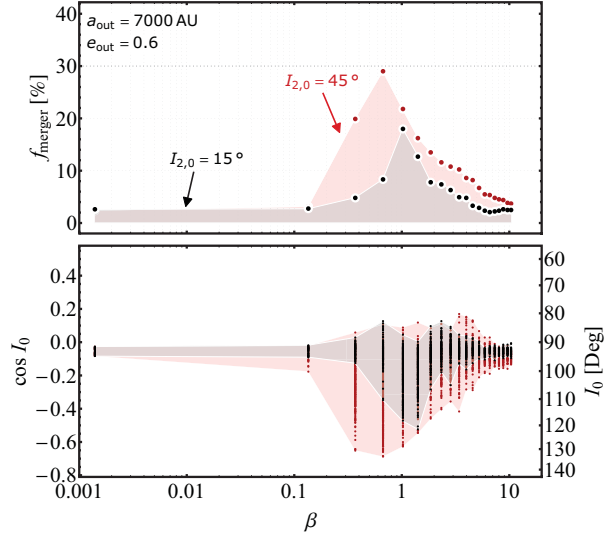


Figure 4. Similar to Figure 3 (the $a_{\text{out}} = 7000\text{AU}$, $e_{\text{out}} = 0.6$ case), except for the initial $I_{2,0} = 15^\circ, 45^\circ$. The β value is evaluated using the initial $I_{2,0}$ (see Equation 34). The black dots correspond to $I_{2,0} = 15^\circ$ and the red dots correspond to $I_{2,0} = 45^\circ$.

Liu & Lai 2018). For the same value of $\bar{a}_{\text{out,eff}}$ (thus the same quadrupole effect), the merger window and merger fraction can be different for different e_{out} . In general, the larger the eccentricity e_{out} , the stronger the octupole effect, and the wider the window. The merger fraction ranges from $\sim 1\%$ (for $e_{\text{out}} \simeq 0$) to a few % (for $e_{\text{out}} = 0.9$). Note that for some values of $\bar{a}_{\text{out,eff}}$, the irregular distribution of merger events inside the merger window is evident; this results from the chaotic behaviors of the octupole-level LK oscillations (see also the examples in Figure 2, particularly the $e_{\text{out}} = 0.6$ case).

For $0.3 \lesssim \beta \lesssim 3$, the merger window and merger fraction are significantly larger for all values of e_{out} . At $\beta \simeq 1$, different values of e_{out} give the similar f_{merger} for each $\bar{a}_{\text{out,eff}}$. The secular resonance enhances f_{merger} to tens of percent.

If the orbital plane of the second inner binary has initially random orientation, LK oscillations in the second binary become possible, and the merger window and merger fraction can be changed. We show an example in Figure 7 for the case of $a_2 = 81\text{AU}$, and the absolute value of $\beta \propto \cos I_2$ is in the range from 0 to 1.18. We see that the merger fraction for the random $\cos I_{2,0}$ case is similar to the $\beta \sim 1$ case depicted in Figures 5-6. However, unlike Figures 5-6, where the window lies in the retrograde regime ($\cos I_0 < 0$), in Figure 7 a large fraction of mergers occurs in the prograde regime ($\cos I_0 > 0$).

Note that the merger fractions presented above are based on the fiducial inner BH binary parameters ($m_1 = 30M_\odot$, $m_2 = 20M_\odot$, $a_0 = 100\text{AU}$). If we start with a closer binary or consider moderately hierarchical systems, where the double-averaged secular approximation may break down, the merger fraction can be even higher (see Liu & Lai 2018).

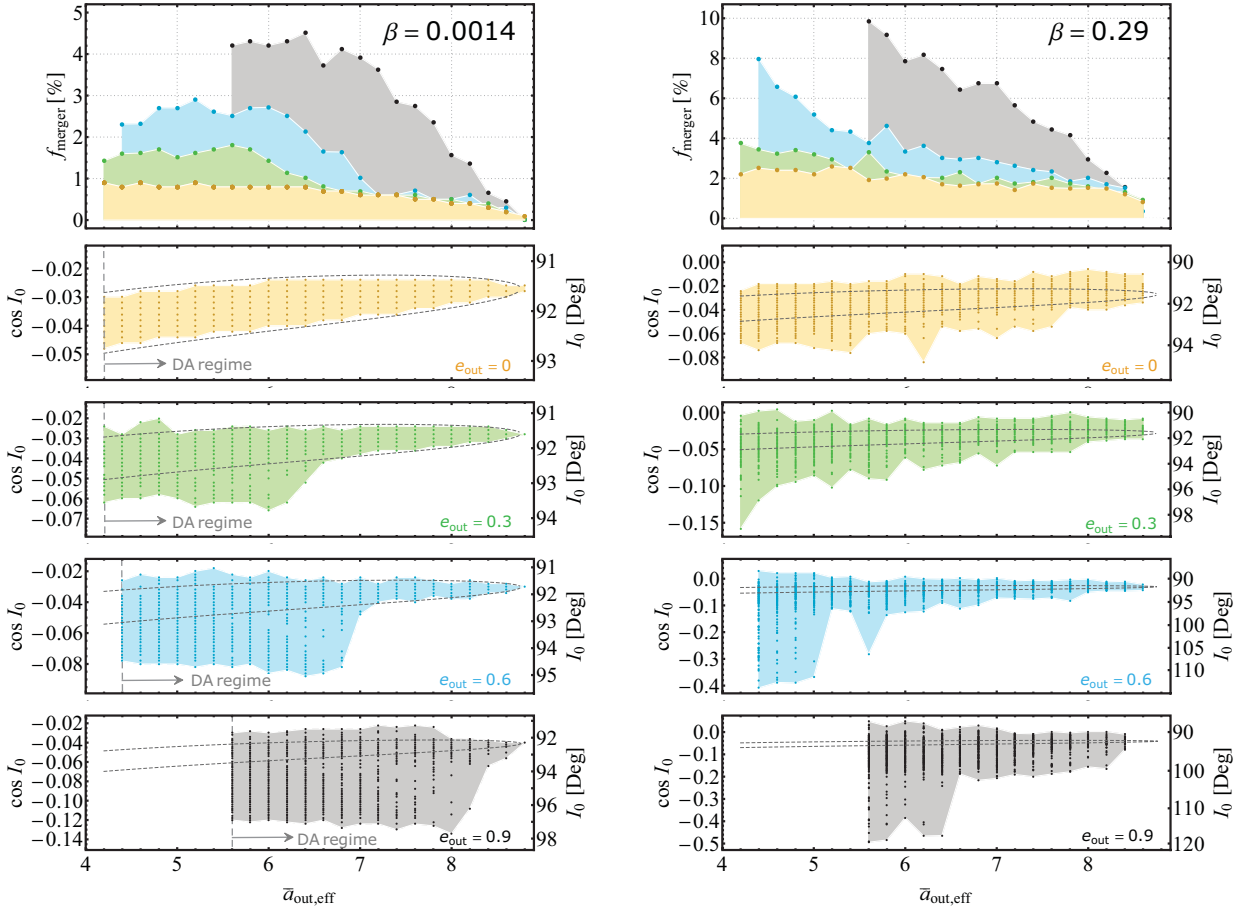


Figure 5. Merger window and merger fraction as a function of the effective semi-major axis of outer binary $\bar{a}_{\text{out,eff}}$ (Equation 27) for $\beta = 0, 0.29$ (corresponding to $a_2 = 1\text{AU}$ and 35AU). Other parameters are the same as the example in Figure 3. In all examples, we assume a fixed $I_{2,0} = 30^\circ$. In each case, each dot (in the bottom four panels) represents a successful merger event within 10^{10} yrs. Note that merger events can have an irregular distribution as a function of $\cos I_0$, because of the chaotic behavior introduced by the octupole terms and binary-binary interactions. Also note that we only consider the range of $\bar{a}_{\text{out,eff}}$ such that double-averaged secular equations are valid (see Equation 26). Different color represents the numerical results from different e_{out} and the shaded areas highlight the boundaries of the merger windows.

Having studied the role of binaries, we now summarize the distribution of the merger time for the merging systems studied in Figures 5-6. We consider systems with $\bar{a}_{\text{out,eff}} \in [5.6, 8.8]$, and assume that the eccentricity of the tertiary companion has a uniform distribution in e_{out} (i.e., $e_{\text{out}} = 0, 0.3, 0.6, 0.9$ are equally probable), and the initial mutual inclination is randomly distributed (uniform in $\cos I_0$). Figure 8 shows the result for four values of β . We see that most systems take long time to merge (with $T_m \sim 10^9 - 10^{10}$ yrs). In particular, a larger fraction of the systems with $\beta \simeq 1$ merge with $T_m > 10^9$ yrs, compared to those with $\beta \ll 1$. This is because when $\bar{a}_{\text{out,eff}} \gtrsim 5.6$, the merger window for systems with $\beta \simeq 1$ is always larger than the other systems ($\beta = 0.0014, 0.29, 1.8$), providing more merger events even with the same quadrupole perturbation (same $\bar{a}_{\text{out,eff}}$).

5 SUMMARY AND DISCUSSION

In this paper, we have studied the mergers of binary BHs induced by the gravitational interaction with tertiary binaries. The binary-binary system is evolved in time using the octupole-level secular equations of motion, taking account of the post-Newtonian effect and gravitational radiation. We examine the dependence of the eccentricity excitation of the BH binary on the orbital properties of the tertiary binary. When the precession timescale of the outer orbit driven by the tertiary binary is comparable to the Lidov-Kozai oscillation time of the BH binary ($\beta \simeq 1$; Equation 34), the LK inclination window for e -excitation is enhanced drastically, leading to more BH mergers compared to the standard triple (“binary + perturber”) systems (see Figure 2).

By conducting a series of numerical integrations, we quantify the role of tertiary binaries in determining the BH merger windows and merger fractions. We find that the orbital properties of the external binary (especially the semi-

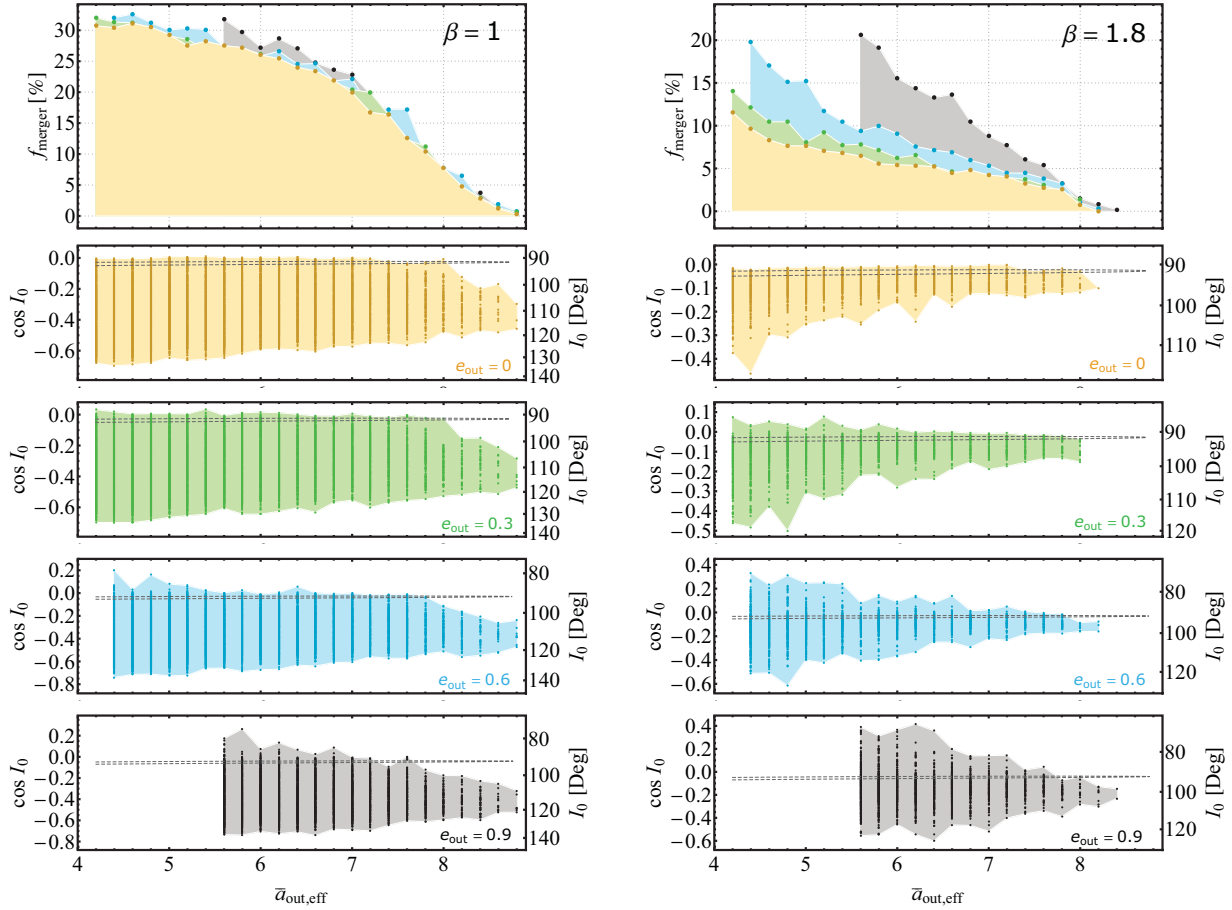


Figure 6. Same as Figure 5, except for $\beta = 1, 1.8$ (corresponding to $a_2 = 81\text{AU}$ and 121AU).

major axis a_2) play a more important role in producing large merger fractions compared to the octupole effect (i.e., eccentric outer orbit). When $\beta \ll 1$ or $\beta \gg 1$, the merger windows are similar as in the standard triples, with the merger fraction less than a few % (see Figure 3). This gives the lower limit of the merger fraction in the binary-binary interaction channel. However, for systems with $\beta \sim 0.3 - 3$, the merger fraction increases to $\gtrsim 10\%$, peaking at $\sim 30\%$, depending on the parameters of the outer orbits (see Figures 5-6). This places the upper limit to the BH merger fraction due to the presence of tertiary binaries. Note that our numerical results are based on the fiducial parameters of first BH binary ($m_{1,2} \simeq 20M_\odot - 30M_\odot$ and initial $a_0 \sim 100$ AU). However, our analysis is not restricted to any specific systems and can be safely extended to other configurations of system parameters. For example, for a relatively compact BH binary, a higher merger fraction induced by the binary-binary interactions could be expected. In triple-driven scenario, similar results can be found in (Liu & Lai 2018).

In this paper we have focused on BH binaries in bound orbits around another binaries. To determine the global BH binary merger rate from such binary-binary channel, we would need to start from a population of main-sequence stellar quadruples, follow them through stellar evolution and

BH formation, and eventually to eccentricity excitation and binary mergers. Such calculation is highly uncertain, and is beyond the scope of this paper. Recent population studies of BH binary mergers from field stellar triples gave a global merger rate of a few per Gpc^3 per year, which is within the low end of the observed BH merger rate determined by LIGO (Silsbee & Tremaine 2017; Antonini et al. 2017). The multiplicity fraction of high-mass main-sequence stars is quite high (as large as 90%), with each star having more than 2 companions on average, suggesting that the stellar quadruple fraction is not much smaller than the stellar triple fraction (Sana 2017). With our finding that the merger fraction of quadruple systems is about 10 times larger than that of triple systems, we conclude that dynamically driven BH mergers in binary-binary systems may be more important than those produced in triple systems, and contribute appreciably to the BH merger events observed by LIGO/VIRGO.

6 ACKNOWLEDGMENTS

This work is supported in part by the NSF grant AST-1715246 and NASA grant NNX14AP31G. BL is also sup-

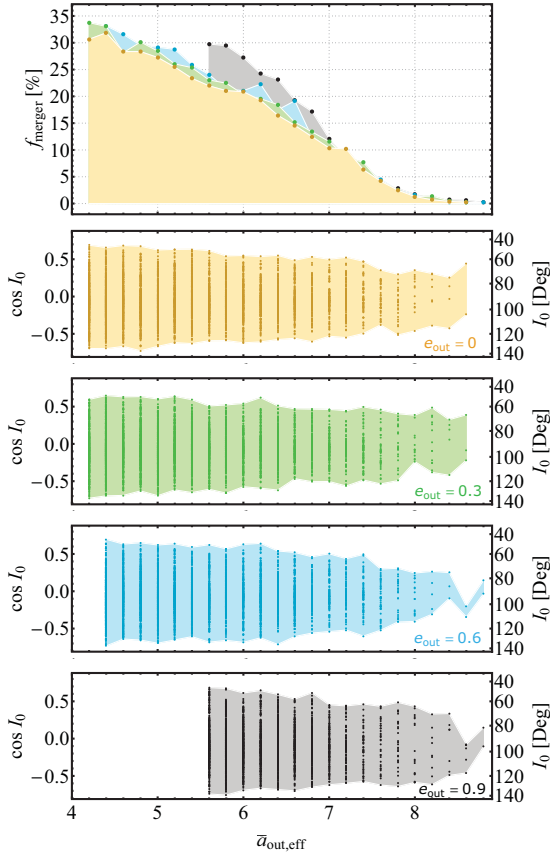


Figure 7. Similar to the case of $a_2 = 81\text{AU}$ in Figure 6, except that the initial $\cos I_{2,0}$ is distributed uniformly in $\cos I_{2,0} \in [-1, 1]$.

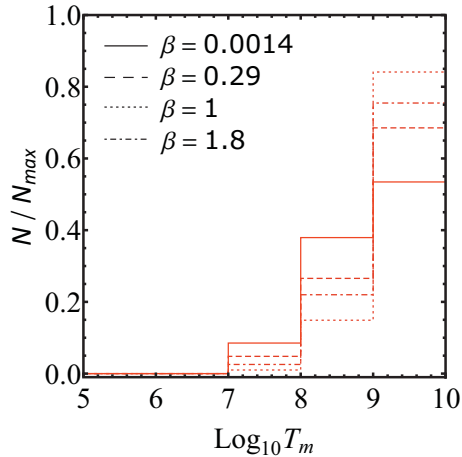


Figure 8. The distribution of merger time (in years) normalized by the number of mergers for different values of β . Here we only include merging systems with $\bar{a}_{\text{out,eff}} \in [5.6, 8.8]$ in Figures 5-6. For each β , the number of mergers is 986 ($\beta = 0.0014$), 1913 ($\beta = 0.29$), 11359 ($\beta = 1$), 3374 ($\beta = 1.8$), respectively.

ported in part by grants from NSFC (No. 11703068 and No. 11661161012). This work made use of the High Performance Computing Resource in the Core Facility for Advanced Research Computing at Shanghai Astronomical Observatory.

REFERENCES

- Abbott B. P., et al., 2016a, *PhRvL*, 116, 061102
 Abbott B. P., et al., 2016b, *PhRvL*, 116, 241103
 Abbott B. P., et al., 2017a, *PhRvL*, 118, 221101
 Abbott B. P., et al., 2017b, *ApJ*, 851, L35
 Abbott B. P., et al., 2017c, *PhRvL*, 119, 141101
 Abbott B. P., et al., 2017d, *PhRvL*, 119, 161101
 Anderson K. R., Lai D., Storch N. I., 2017, *MNRAS*, 467, 3066
 Antonini F., Perets H. B., 2012, *ApJ*, 757, 27
 Antonini F., Murray N., Mikkola S., 2014, *ApJ*, 781, 45
 Antonini F., Rasio F. A., 2016, *ApJ*, 831, 187
 Antonini F., Toonen S., Hamers A. S., 2017, *ApJ*, 841, 77
 Banerjee S., Baumgardt H., Kroupa P., 2010, *MNRAS*, 402, 371
 Belczynski K., Dominik M., Bulik T., O’Shaughnessy R., Fryer C., Holz D. E., 2010, *ApJ*, 715, L138
 Belczynski K., Holz D. E., Bulik T., O’Shaughnessy R., 2016, *Natur*, 534, 512
 Chatterjee S., Rodriguez C. L., Kalogera V., Rasio F. A., 2017, *ApJ*, 836, L26
 Dominik M., Belczynski K., Fryer C., Holz D. E., Berti E., Bulik T., Mandel I., O’Shaughnessy R., 2012, *ApJ*, 759, 52
 Dominik M., Belczynski K., Fryer C., Holz D. E., Berti E., Bulik T., Mandel I., O’Shaughnessy R., 2013, *ApJ*, 779, 72
 Dominik M., et al., 2015, *ApJ*, 806, 263
 Downing J. M. B., Benacquista M. J., Giersz M., Spurzem R., 2010, *MNRAS*, 407, 1946
 Fang X., Thompson T. A., Hirata C. M., 2018, *MNRAS*, 476, 4234
 Hamers A. S., Portegies Zwart S. F., 2016, *MNRAS*, 459, 2827
 Hamers A. S., Lai D., 2017, *MNRAS*, 470, 1657
 Hamers A. S., 2018, *MNRAS*, 478, 620
 Hamers A. S., Bar-Or B., Petrovich C., Antonini F., 2018, *arXiv*, arXiv:1805.10313
 Hoang B.-M., Naoz S., Kocsis B., Rasio F. A., Dosopoulou F., 2018, *ApJ*, 856, 140
 Kozai Y., 1962, *AJ*, 67, 591
 Leigh N. W. C., et al., 2018, *MNRAS*, 474, 5672
 Li G., Naoz S., Holman M., Loeb A., 2014, *ApJ*, 791, 86
 Lidov M. L., 1962, *Planet. Space Sci.*, 9, 719
 Lithwick Y., Naoz S., 2011, *ApJ*, 742, 94
 Lipunov V. M., Postnov K. A., Prokhorov M. E., 1997, *AstL*, 23, 492
 Lipunov V. M., et al., 2017, *MNRAS*, 465, 3656
 Liu B., Muñoz D. J., Lai D., 2015, *MNRAS*, 447, 747
 Liu B., Lai D., 2018, *ApJ*, 863, 68

- Mandel I., de Mink S. E., 2016, MNRAS, 458, 2634
Marchant P., Langer N., Podsiadlowski P., Tauris T. M.,
Moriya T. J., 2016, A&A, 588, A50
Mardling R. A., Aarseth S.J., 2001, MNRAS, 321, 398
Miller M. C., Hamilton D. P., 2002, ApJ, 576, 894
Miller M. C., Lauburg V. M., 2009, ApJ, 692, 917
Naoz S., 2016, ARA&A, 54, 441
O’Leary R. M., Rasio F. A., Fregeau J. M., Ivanova N.,
O’Shaughnessy R., 2006, ApJ, 637, 937
O’Leary R. M., Kocsis B., Loeb A., 2009, MNRAS, 395,
2127
Pejcha O., Antognini J. M., Shappee B. J., Thompson
T. A., 2013, MNRAS, 435, 943
Peters P. C., 1964, PhRv, 136, 1224
Petrovich C., 2015, ApJ, 799, 27
Petrovich C., Antonini F., 2017, ApJ, 846, 146
Podsiadlowski P., Rappaport S., Han Z., 2003, MNRAS,
341, 385
Portegies Zwart S. F., McMillan S. L. W., 2000, ApJ, 528,
L17
Rodriguez C. L., Morscher M., Pattabiraman B., Chatter-
jee S., Haster C.-J., Rasio F. A., 2015, PhRvL, 115, 051101
Sana H., 2017, IAUS, 329, 110
Samsing J., D’Orazio D. J., Askar A., Giersz M., 2018,
arXiv, arXiv:1802.08654
Seto N., 2013, PhRvL, 111, 061106
Silsbee K., Tremaine S., 2017, ApJ, 836, 39
Thompson T. A., 2011, ApJ, 741, 82
VanLandingham J. H., Miller M. C., Hamilton D. P.,
Richardson D. C., 2016, ApJ, 828, 77
Vokrouhlický D., 2016, MNRAS, 461, 3964
Wen L., 2003, ApJ, 598, 419